1st IAA Conference on Space Situational Awareness (ICSSA)

Orlando, FL, USA

IAA-ICSSA-17-01-01
UNCERTAINTY TREATMENT IN THE GOCE RE-ENTRY

Edmondo Minisci[(1)], **Romain Serra**[(1)], **Massimiliano Vasile**[(1)], **Annalisa Riccardi**[(1)], **Stuart Grey**[(1)], **Stijn Lemmens**[(2)]

[(1)] *University of Strathclyde, 75 Montrose St, Glasgow, UK, edmondo.minisci@strath.ac.uk*

[(2)] *ESA/ESOC Space Debris Office (OPS-GR), Robert-Bosch-Str. 5, 64293 Darmstadt, Germany, stijn.lemmens@esa.int*

Keywords: *Re-Entry Analysis, Uncertainty Treatment, GOCE*

This paper presents the work to characterize and propagate the uncertainties on the atmospheric re-entry time of the Gravity field and steady-state Ocean Circulation Explorer (GOCE) satellite done with the framework of an ESA ITT project. Non-intrusive techniques based on Chebyshev polynomial approximation, and the Adaptive High Dimensional Model Representation multi-surrogate adaptive sampling have been used to perform uncertainty propagation and multivariate sensitivity analyses when both 3 and 6 degrees-of-freedom models where considered, considering uncertainties on initial conditions, and atmospheric and shape parameters. Two different uncertainty quantification/characterization approaches have been also proposed during the project. The same interpolation techniques used for non-expensive non-intrusive methods for uncertainty propagation, allowed the development of two methods based on direct optimization approaches, the Boundary Set Approach and the Inverse Uncertainty Quantification. Moreover, an innovative approach to treat the empirical accelerations has been proposed, based on polynomial expansions in the state variables. The method has been tested and further developed to consider uncertainties in the initial conditions, leading to a statistical characterization of the coefficients and representation of the possible trajectories. Finally, the investigation on the use of meta-modeling techniques to directly map a range of initial conditions and model uncertainties, as well as characteristics of the considered object, into the parameters of the skew-normal distribution that usually characterizes the re-entry time windows, bringing to a very fast characterization of the output PDF not requiring any further propagation at all, is also briefly described.

1. Introduction

The Gravity field and steady-state Ocean Circulation Explorer (GOCE) satellite, operated at very low altitude by the European Space Agency (ESA), ran out of propellant on October 21 2013, triggering a fast orbit decay eventually leading to its disintegration in the atmosphere three weeks later on November 11. While its primary mission was to study the Earth's gravitational field, its end-of-life trajectory was intensively studied

in an effort to document atmospheric re-entry in order to better understand and predict it. During the three weeks period between the end-of-mission and the re-entry of the ESA GOCE vehicle, orbital data collection resulted in a rich set of data from which to improve the understanding of the uncertainties associated with the re- entry process. Knowledge of the position and attitude of the GOCE vehicle during this period, allied to understanding of the aerodynamics of the vehicle and behavior of the atmosphere, can provide new insight into the processes which drive the uncertainties in the prediction of re-entry timing. In collaboration with SpaceDyS Srl and Belstead Research Limited (BRL), the University of Strathclyde has been awarded an ITT project to exploit these data. Whereas the two industrial partners have been focusing respectively on orbit determination and aerodynamic behavior of the 'Ferrari of space', the academic one has been responsible for the treatment of uncertainty.

In re-entry prediction, uncertainty lies in the initial orbit estimation as well as the model parameters for examples the ones related to the atmosphere. The standard Monte Carlo method represents a somehow brute-force approach to uncertainty propagation, as the required amount of simulations can lead to unreasonable computational times, especially when the number of uncertain variables is high. On the other hand, first-order methods focus on the propagation of the covariance matrix to estimate the dispersion on the final state. However, it is argued that they provide information only on the first two statistical moments. This issue can be overcome by using high-order approximations of the function of interest, here the re-entry time, as it is now more and more done in the field of aerospace engineering. Nonlinear surrogates are computable for instance with polynomial expansions. They can be performed either intrusively, as is the case for the Taylor differential algebra [1], or not i.e. treating the function of interest as a black-box, for example with polynomial chaos when dealing with Gaussian variables [12]. A different approach is the so-called Adaptive High-Dimensional Model Representation (AD-HDMR), a non-intrusive method originating from the fluid dynamics community that focuses on interactions between the random variables [4, 5]. In short, this method decomposes the stochastic space into sub-domains of lower dimensionality, and models each sub-domain with the most appropriate technique. Then the overall model is built by summation of the contributions of each sub-domain.

At the University of Strathclyde, several of these modern quantification techniques have been applied to the uncertainty in GOCE's end-of-life trajectory. Hence, a comparison between intrusive polynomial expansions has been performed [8]. More precisely, Chebyshev and Taylor approaches were used to simulate GOCE's orbit decay, demonstrating the robustness of the former over the latter. In parallel, two non-intrusive techniques have been utilized and it is the work based on these approaches that is reported here. On one hand, a non-intrusive version of multivariate Chebyshev polynomials was used in an effort to characterize the uncertainty region leading to a given time-window (Boundary Set Approach) or probability distribution function of the re-entry time (Inverse Uncertainty Quantification). On the other hand, the HDRM method has been extensively used to approximate probabilistic distributions of re-entry times, enabling the generation of a large database and setting the path to an artificial intelligence approach for re-entry predictions. Moreover, an innovative method to treat the empirical accelerations has been proposed, based on polynomial expansions in the state variables. It has been tested and further developed to consider uncertainties in the initial conditions, leading to a statistical characterization of the coefficients and

representation of the possible trajectories.

This paper is organized as follows: Section 2 describes some of the uncertainty analyses performed on GOCE's re-entry using surrogates and Monte Carlo runs; Section 3 describes the works done to develop and test some proposed techniques for the characterization of the input uncertainties; Section 4 describes the proposed innovative approach to treat the empirical accelerations; Section 5 builds on some of the outcomes of Section 2 and describes some of the analysis performed to test the application of computational intelligence to the problem of re-entry prediction, by learning a database of probabilistic distributions from a campaign of simulated trajectories; and a Section of Conclusions ends the paper. Note that two different trajectory propagators have been used throughout this work: BRL's aero-thermal simulator for the results reported in Sections 2 and 3, while in the rest of the paper it is an in-house code developed at Strathclyde University.

2. Uncertainty quantification in GOCE's re-entry

In this Section, some of the results on the uncertainty propagation analyses carried out during the project are reported. Non intrusive and intrusive UP methods have been used to propagate the uncertainties on the initial states (position, velocity, attitude and attitude rates), and atmospheric and shape parameters, such as a density multiplier that represents both the multiplicative uncertainties on the drag coefficient, C_D, and on the modeled density, the logarithmic geomagnetic index, Kp, and the solar flux index, $F10.7$. For the sake of simplicity, random input variables corresponding to the considered uncertainties have all been considered as uniformly distributed in this study. The non intrusive methods were coupled to the re-entry simulations code of BRL.

2.1. Non-intrusive surrogates

The most general way to perform uncertainty propagation (UP), as well as global sensitivity analysis, is to use the Monte-Carlo (MC) approach, which basically follows three main steps:

1. sample the input random variable(s) from their known or assumed (joint) Probability Density Function (PDF),
2. compute deterministic output for each sampled input value(s), and
3. determine the statistical characteristics of the output distribution (e.g. mean, variance, skewness).

The MC method has the property that it converges to the exact stochastic solution when the number of samples $n \to \infty$. In practice the value of n can be a finite number, but to have a highly converged process it should be very high, causing an excessive computational costs (even for modern computers). A way to reduce the computational time of the UP process could be to build a less expensive surrogate of the model and then use it to propagate the uncertainty. Two different approaches have been used for this work, as described in what follows.

2.1.1. Chebyshev interpolation

One of the non-intrusive approaches used here is the multivariate Chebyshev interpolation. In short, the model is sampled on the interval of interest, using points generated randomly via a latin hypercube sampling. These so-called nodes are then

used to compute the coefficients of the Chebyshev polynomial. The degree of the latter fixes the minimum number of samples required, which also depends on the dimension of the problem. If more samples are provided, the system becomes overdetermined and a least square approach is used to derive the coefficients. In any case, the output is a multivariate polynomial, written in the Chebyshev basis, that approximates the function of interest at a given order. More details on this method can be found in [9] for example.

2.1.2. AD-HDRM

The AD-HDMR approach proposed for this study is based on the cut-High Dimensional Model Representation (cut-HDMR) decomposition, and it allows a direct cheap reconstruction of the quantity of interest and analyses similar to an ANOVA (Analysis Of Variance) decomposition. Basically, the function response (the re-entry time in this case) is decomposed in a sum of contributions given by each stochastic variable and each one of their interactions through the model, considered as increments with the respect the nominal response, f_c:

$$f(x) = f_c + \sum_{i}^{n} dF_i + \sum_{1 \le i < j \le n} dF_{ij} + ... + dF_{1,...,n}$$

where n is the number of variables. A surrogate model representation can be independently generated for each element of the sum (called Increment Functions) and only for the non- zero elements, thus greatly reducing the complexity of sampling and building the model. Moreover, the contribution of each term of the sum to the global response can be quantified independently so that higher order interactions with low or zero contribution can be neglected already by analyzing the lower order terms.

Not only is the output of this method the (multi-dimensional) distribution of the quantity of interest, but also the quantification of the global contribution of each term of the sum to the global response. This feature, allows for a complete analysis of the sensitivity of the response with respect to each of the stochastic variables, as well as their interactions. Moreover in the case that the objective function should be considered as a black box, the analysis of the single contributions can give an insight into the structure of the response function.

Moreover, an adaptive sampling technique, which compares the interpolation process in each iterative step, is also used. The position of a new sample is then given by the largest difference between these two interpolations, where the difference is computed as the change of a shape of the selected interpolation technique. The selected interpolation technique is the so called Multi-surrogate adaptive technique, which is able to combine and exploit various interpolation techniques. The convergence process of the adaptive part is based on the observation of the statistical properties of the weight function propagated through the interpolation technique.

2.2. 6 degrees-of-freedom analysis

PDF obtained from simulations taking into account attitude are multi-modal and do not happen to match real data acquired on GOCE's re-entry. The reason for this is that the spacecraft, as modeled with the 6DoF propagator and unlike the actual vehicle, does not have its attitude controlled. As a result, in the numerical simulation, it remains aerodynamically unstable at the beginning of the orbit decay, before stabilizing towards

the last few days. The time variability in this transition then creates different re-entry windows which in turn cause this particular distribution of the final uncertainty, as seen in Figure 1((1)), where the re-entry time distribution from initial conditions on Day 20 is shown. The distribution is obtained by MC sampling (1.80e5 samples) and it can be seen that the high number of samples allows to visualize some structure of the PDF that cannot be really detected with a small amount of samples: multiple peaks visible in the Figure 1((2)), cannot be detected with the large bins used for Figure 1((1)).
Uncertainty ranges are:

- Initial position (Earth-Centered Earth-Fixed): ± 0.5 km
- Initial velocity (ECEF): ± 0.5 m/s
- Density multiplier: ± 0.03
- Geomagnetic index: ± 1
- Solar flux: ± 10^{-22} $W/(m^2 Hz)$

The nominal re-entry time is 2.28 [day], and the re-entry time window obtained from the 1.8e5 samples of the MC simulations is [1.93, 2.8] [day], resulting in a T_{wR}= [-15.4, + 22.9] %.
The real extremes of the re-entry time interval (indicated by the red vertical lines in Figure 1((2))) have been found by means of an optimization process that used the 6DOF model as a black-box. The 6DOF model has been coupled with an evolutionary based algorithm (the Adaptive Inflationary Differential Evolution Algorithm, AIDEA [6]) and two optimization processes have been performed. In the first process, the space of uncertainties has been explored to find the minimum of the re-entry time, while in the second one, the optimizer searched for the maximum of the re-entry time. Both processes required near 3000 model evaluations (i.e., numerical propagations) each to converge to the optimal solutions (the extreme points of the distribution). The re-entry time window obtained from the optimization processes is [1.86, 2.98] [day], resulting in a T_{wR} = [-18.4, + 30.7] %

Another study [2, 10] by the authors on drag sails, also conducted in collaboration with BRL, confirms it by showing that PDF become unimodal if a single regime (stable or pure tumbling) lasts during most of the re-entry. Moreover, it has been observed that, under these conditions, 3DoF distributions can match relatively well their 6DoF counterparts, hence allowing for a significant gain in computational cost for re-entry prediction. This is illustrated by Figure 2 that compares PDFs obtained with different degrees-of-freedom for the same vehicle. Since the 3DoF one does not simulate attitude, note that the matching is achieved by tuning the ballistic coefficient of the equivalent sphere.

2.3. 3 degrees-of-freedom analysis

Due to the cannonball assumption, PDF from 3DoF simulations of GOCE are not affected by aerodynamic stability and do not appear to be multi-modal. Furthermore, several analytical distributions have been proposed to fit the data: normal, skew normal, lognormal and Weibull. In this case, the parameters of the fitting skew normal have been found by means of an optimization process, using the evolutionary algorithm IDEA. Normal, lognormal, and Weibull distributions fitting the data have been obtained via built-in ©Matlab functions.

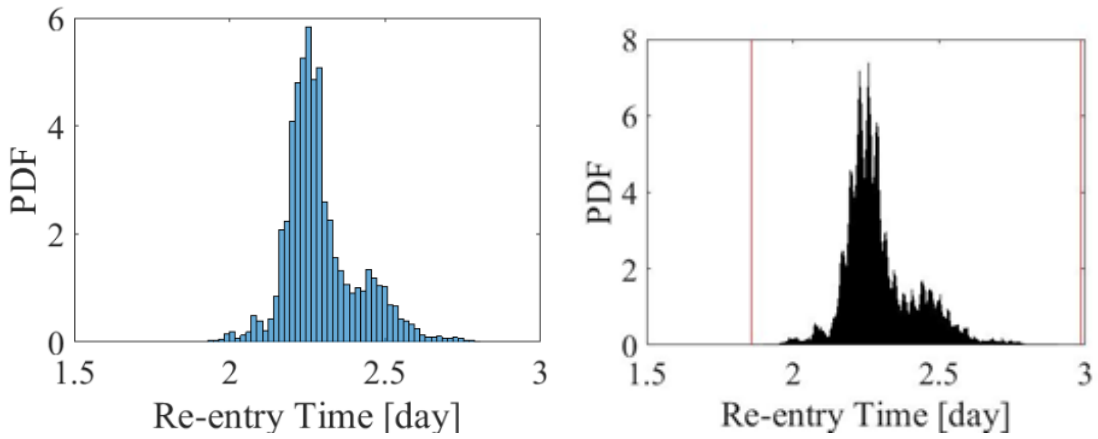

((1)) Coarse ((2)) Fine

Figure 1: Re-entry time distribution for propagation from Day 20 initial conditions by 6DOF: 1) coarse resolution of the histogram and 2) fine resolution of the histogram obtained via MC sampling

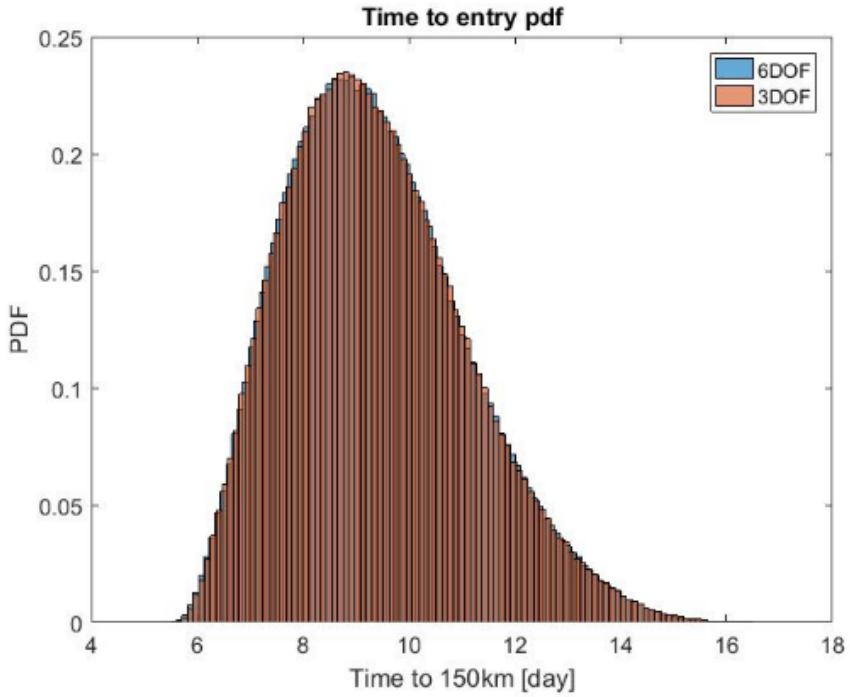

Figure 2: Comparison between 3 and 6DoF PDFs for the re-entry time of a drag sail

Among these laws, the skew normal seems to be the best regression model. An example can be seen on Figure 3 where, in red, it clearly performs better than the others on the peak and right-hand side of the original distribution, pictured in green. The accuracy is not as good on the left part of the tail, but this is due to the mathematical

definition of the probabilistic law itself. Indeed, its PDF ϕ is:

$$\begin{aligned} \phi(x) : (-\infty, +\infty) &\mapsto (0, +\infty) \\ x &\mapsto \frac{1}{\pi\omega} \exp\left(-\frac{(x-\xi)^2}{2\omega^2}\right) \int_{-\infty}^{\alpha(\frac{x-\xi}{\omega})} \exp\left(-\frac{t^2}{2}\right) \mathrm{d}t, \end{aligned} \tag{1}$$

where ξ is the location, ω the scale (positive) and α the shape. Thus, the support of ϕ is not limited to positive values while, in contrast, re-entry times cannot be negative. As a result, the skew normal law is bound to have poorer results on the left-hand side of the distribution, if only because it artificially introduces re-entry times smaller than zero. Nonetheless, it can be seen from the figure that its overall performance is better than the normal, lognormal, and Weibull models, and the values of the fitting performance index confirm it.

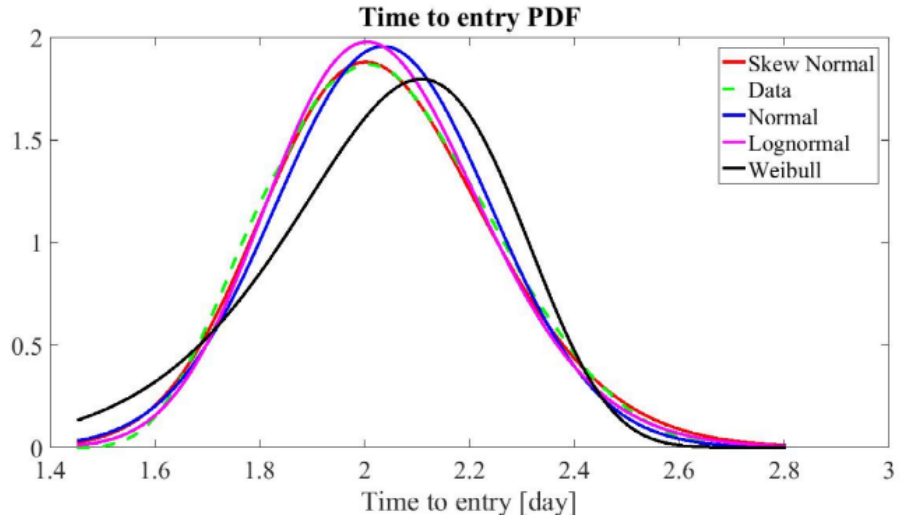

Figure 3: Comparison between data and fitting models

3. Uncertainty characterization approaches

In this section, different methods and approaches to quantify and characterize the uncertainties are described and some results are shown and commented.

3.1. Boundary Set Approach

Given a trust-interval $\mathcal{I}$ on the re-entry time, the boundary set approach derives the largest ellipsoid such that all occurrences of the uncertain parameters contained in this region lead to a re-entry time within the desired bounds. Instead of the full orbit propagator, which is computationally intense to run, its non-intrusive Chebyshev surrogate is used to evaluate the re-entry time. The computation of the ellipsoid is done in three major steps. First, a series of optimization problems is solved in order to find points on the boundary i.e. where the re-entry time reaches the fixed limits. Then a principal-axis analysis is performed on this set of points. The result determines the axis and aspect ratios of the final ellipsoid. The last step consists in an iterative search for the largest possible size of this ellipsoid. In the following, the method is detailed and illustrated on a simple 2-D test-case in order to visualize things. This

example simulates GOCE's trajectory with 3DoF dynamics from 03:00:00 on 9/11/13 (Day 20 case) until re-entry at 80km. Only two uncertain parameters are considered: initial speed (±2 m/s w.r.t. nominal) and atmospheric density (±10% w.r.t. nominal). All other variables in the model are assumed to be deterministic and set to nominal values. A Chebyshev polynomial of degree 3 is computed non-intrusively as a surrogate for re-entry time by means of a sparse interpolation with 65 calls to the orbit propagator (see Figure 4). The trust-interval $\mathcal{I}$ is set to 174870.02s ±10%.

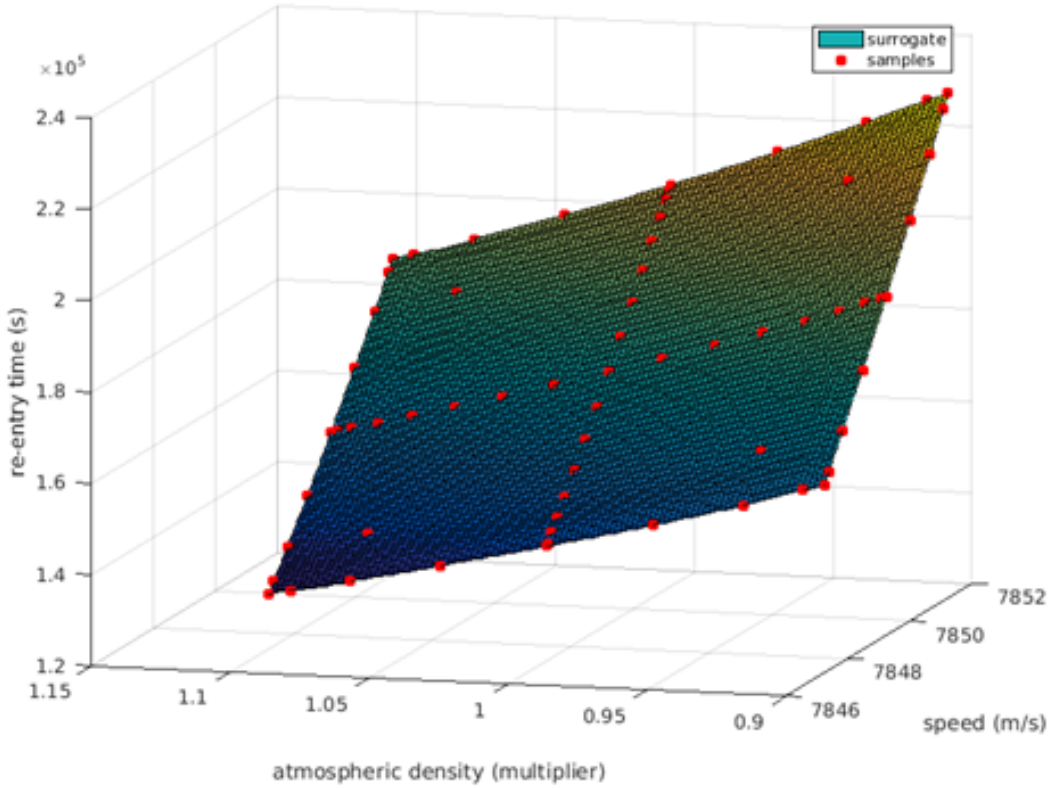

Figure 4: Non-intrusive Chebyshev surrogate for 2-D test-case

3.1.1. Finding boundary points

By definition, the boundary set contains all points in the uncertain region where the re-entry time reaches the limits of the desired interval. In order to locate those points, a series of maximization problem in one dimension is solved. For each of them, as a start, a search direction $\mathbf{D}$ is randomly generated. Then, initialized at the nominal point x_0, the optimizer tries to find the farthest point away from it such that re-entry time is still in the trust-interval. It can be formulated as follows:

$$\begin{aligned} &\max |y| \\ &s.t. \quad T_R(\mathbf{x}_0 + y\mathbf{D}) \in \mathcal{I} \end{aligned} \tag{2}$$

where T_R is the time of re-entry function. If the optimization fails for some reason, the result is discarded. If the algorithm converges, the point is saved.

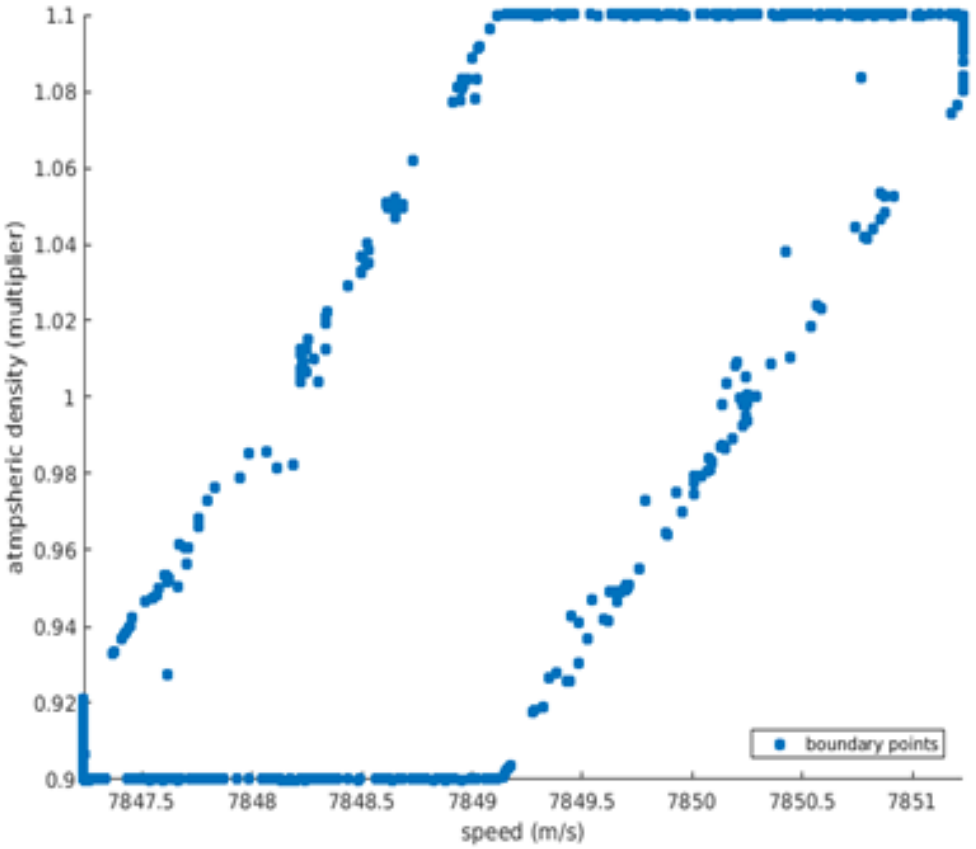

Figure 5: Results from the search for boundary points

Using the present test-case, 1000 optimization problems were run, leading to 484 saved points shown in blue in Figure 5. The upper-left corner is the region where re-entry time is too short while the lower-right one corresponds to re-entry times that are too long.

3.1.2. Modeling the shape of the ellipsoid

Now that an approximation of boundary points has been generated, the idea is to somehow model them with a classical shape. A geometry of choice is an ellipsoid, since it is of use for Gaussian probability distributions. Thus, given the points found in the previous step, a principal-axis analysis is performed with ©Matlab built-in functions. The aspect ratios of the ellipsoid can also be deduced from this analysis. However, it is not assured that all points inside an ellipsoid with this shape are within the trust-interval $\mathcal{I}$. How to find the right size is addressed in the final step. For this 2-D test-case, the eigenvectors are (0.99877,0.04949) and (-0.04949,0.99877) while the eigenvalues are 1.5919 and 0.0032, giving an aspect ratio of 0.002.

3.1.3. Tuning the size of the ellipsoid

The axis and aspect ratios previously computed determine the shape of the ellipsoid. The only free parameter left is the size. In order to find it, an iterative search is performed. The initialization starts with an arbitrary length and samples within the ellipsoid to check where re-entry times spread. The sampling is performed assuming

a Gaussian probability distribution. If all the samples are in-range, the next iteration increases the size of the ellipsoid, if not, it reduces it, until a stopping criterion is reached. In summary, it is a simple process of dichotomy.

Figure 6 depicts the initialization where the ellipsoid contains out-of-range points. The result of the iterative search is shown in Figure 7. It can be seen that no samples are out-of-range (no red point).

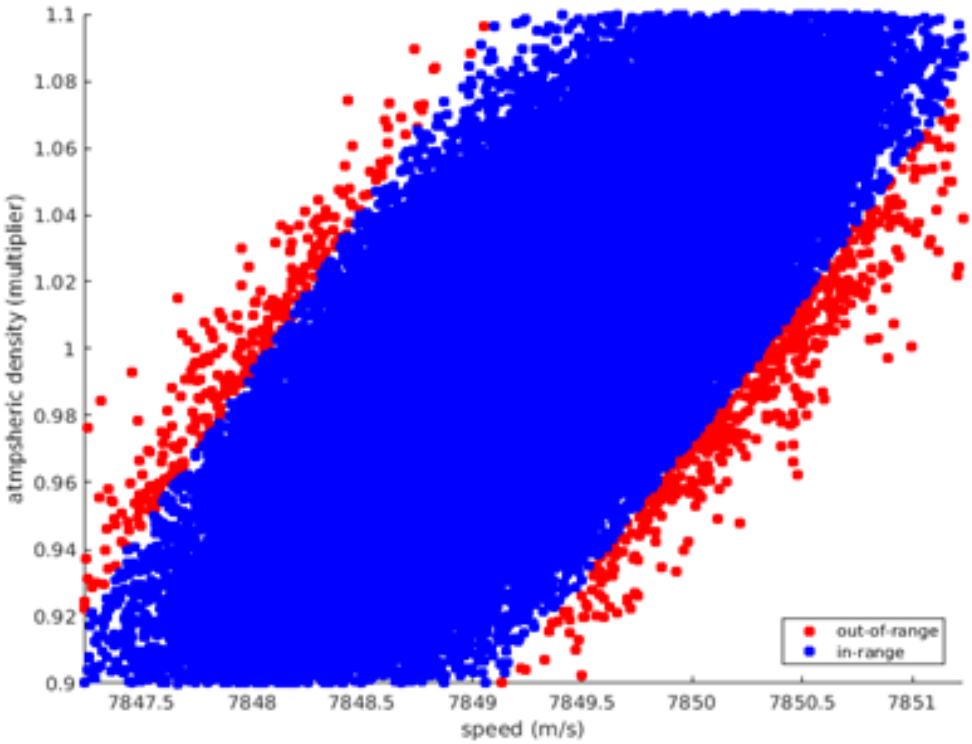

Figure 6: Results of initial Gaussian sampling

The generalization of this approach to N dimensions is rather straightforward, although results cannot be visualized as in 2-D. In the first step, since the search for boundary points is done in given directions, there is no increase in the number of optimizations variables, which remains one for each problem. Then, the principal-axis analysis can be performed without any issue in dimension N. Finally, the search for the largest possible size for the ellipsoid is done by sampling multi-normal laws in N-D instead of 2-D.

A few 2-D projections of ellipsoids obtained with $N = 9$ are given next. More precisely, the model consists of a 3DoF propagation with uncertain parameters being the initial conditions (6 components) as well as the atmospheric parameters (density multiplier, geomagnetic index and mean solar flux). Once again, the simulation starts at 03:00:00 on 9/11/13 and runs until re-entry at 80km. The following projections focus on the same variables than before: speed and density multiplier. First is shown the second last sampling before the iterations stop (Figure 8). One can still see red spots among the samples, meaning that some violate the range-constraint on re-entry time. The second projection (Figure 9) show the final sampling, where no point is out-of-range.

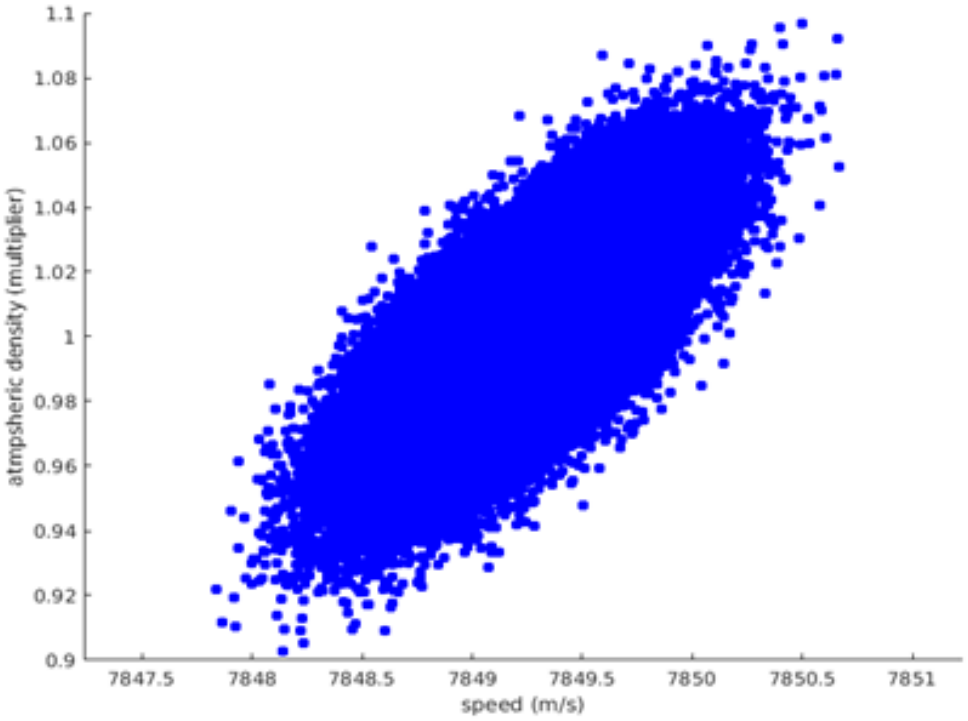

Figure 7: Results of final Gaussian sampling

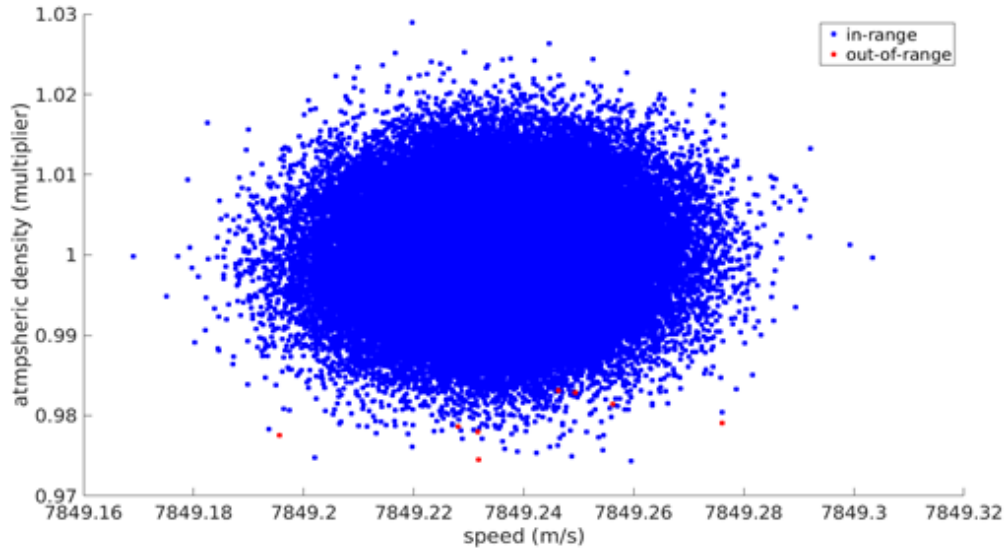

Figure 8: 2D projection of second last sampling

In conclusion, this approach is a way of finding ellipsoidal sets where bounds on the time of reentry are satisfied. It could be used for instance to initialize inverse problems such as the one presented thereafter.

3.2. Inverse Uncertainty Quantification

The goal of this section is to describe how the inverse propagation approach works and give an idea of the potentialities. Given a probabilistic distribution for the time of re-

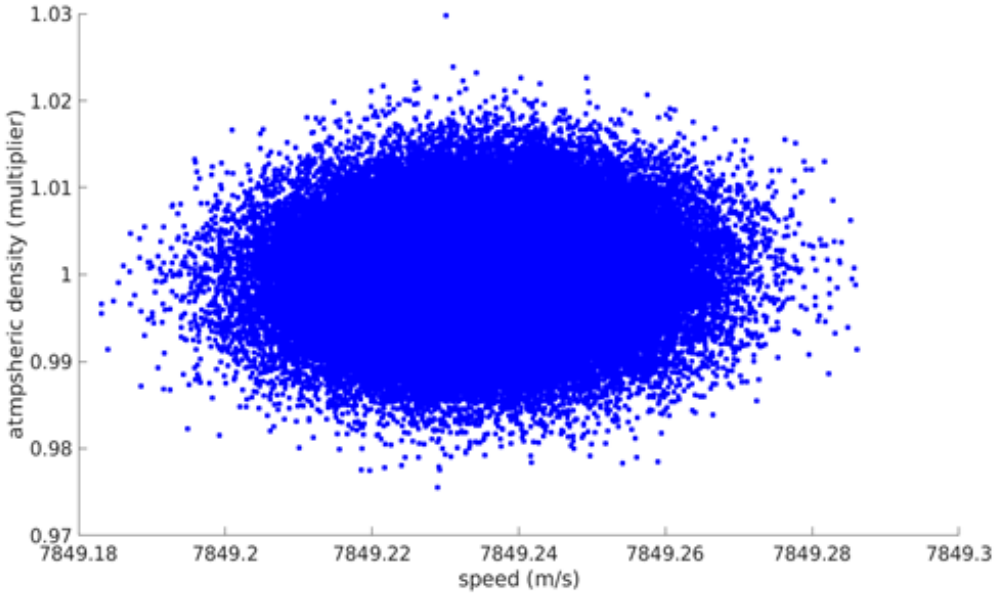

Figure 9: 2D projection of last sampling

entry, the approach lets to infer the structure of the corresponding input distributions. This is done through an optimization process, which minimizes the difference between the required output distribution and the output distribution obtained by the propagation of the parametrized input uncertainties.

In this particular case, the parametrization of the input distributions is done via a kernel approach. More precisely, the initial probability density function of each input uncertainty is assumed to be a superposition of M kernels, with the same variance but with different mean values. Using the parameters of the kernel as optimization variables, the inverse problem can be cast as a minimization problem of dimensionality $d = n_i(M + 1)$, where n_i is the number of input uncertainties.

Solving this optimization problem using the real model i.e. the full orbit propagator to generate the output distribution would be too costly, so a surrogate is used instead. In this work, the surrogate is obtained via the non-intrusive Chebyshev approach.

In what follows, the results for four different test cases (different input parameterizations), when input uncertainties affect the a) initial Day 20 ECEF position components , b) initial Day 20 ECEF velocity components, c) multiplicative density parameter, d) geomagnetic index Kp, e) mean flux density $F10.7$, are shown.

For the first case uniform distributions are used, while for all the other three cases epanechnikov kernels are used. The re-entry time is constrained between 0.8 and 1.2 of the nominal re-entry time, that is [1.62, 2.43] (day).

3.2.1. Case 1

Uniform distribution centered in the nominal value for each one of the 9 input uncertainties. In this case, without any constraints, the optimal solution is:

- $r_1 : \pm 10^{-6}\ m$; $r_2 : \pm 10.986\ m$; $r_3 : \pm 1840.1\ m$
- $v_1 : \pm 10^{-6}\ m/s$; $v_2 : \pm 10^{-6}\ m/s$; $v_3 : \pm 10^{-6}\ m/s$
- Dens. mult.: $\pm 10^{-6}$; $Kp : \pm 10^{-6}$; $F10.7 : \pm 10^{-6} sfu$

Basically the optimizer finds that the best solution to have a quasi uniform distribution for the re-entry time is to have a non-null uncertainty only on one of the position components.

3.2.2. Case 2

In this case, 1 single kernel is used for each one of the 9 input uncertainties. Kernels are free to float, then cannot be considered as proper uncertainties. The case is just to show how the method works. The optimal kernels are shown in Figure 10, while the optimal result is shown in Figure 11. One single kernel is not enough to have a uniform distribution, as requested.

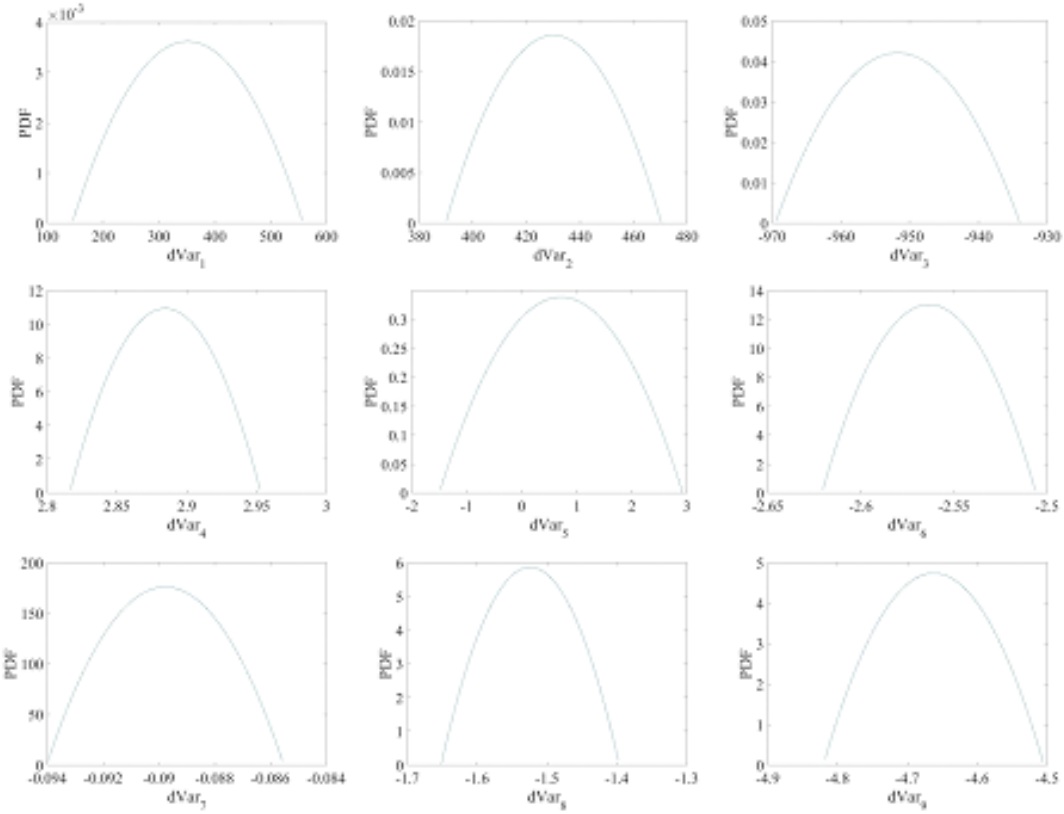

Figure 10: Optimal input distributions for Case 2 inverse propagation (one single kernel for each input variable)

3.2.3. Case 3

In this case, 2 kernels are used for each one of the 9 input uncertainties. Again, kernels are free to float and cannot be considered as proper uncertainties, but it possible to see, that compared to the previous case, an optimal use of the kernels (Figure 12) leads to a much uniform distribution for the output (Figure 13).

3.2.4. Case 4

This is a more realistic case: two kernels are used for each one of the 9 input uncertainties, but this time the kernels are not free to float, and are constrained to include the nominal value. The optimal kernels are shown in Figure 14, while the optimal result is shown in Figure 15.

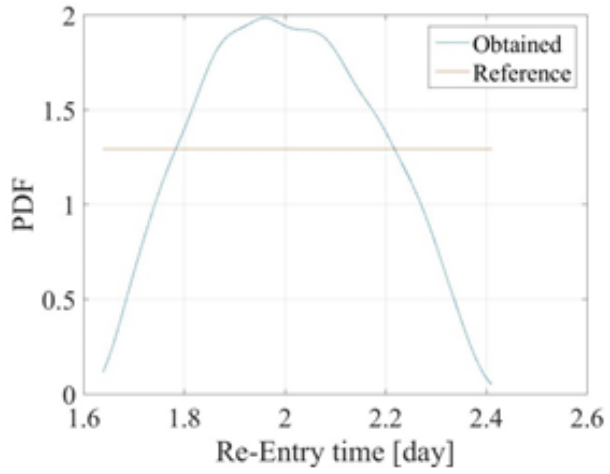

Figure 11: Re-entry time distribution for Case 2

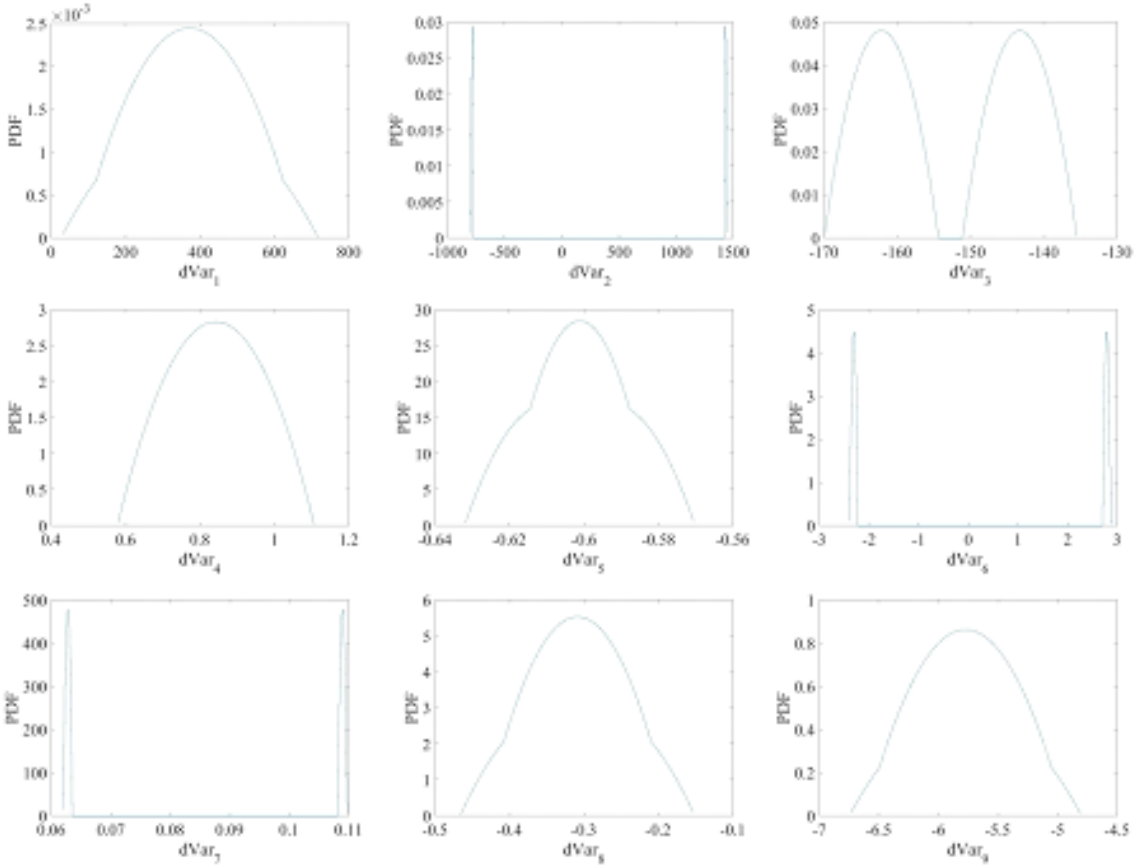

Figure 12: Optimal input distributions for Case 3 (two kernels for each input variable)

4. Empirical acceleration

Non-modeled terms in a dynamical system can be incorporated in a so-called empirical way. Typically, it consists of introducing functions defined by a number of parameters that are somehow fitted so that the propagated state matches the actual measurements. The technique proposed here consists in using polynomials as func-

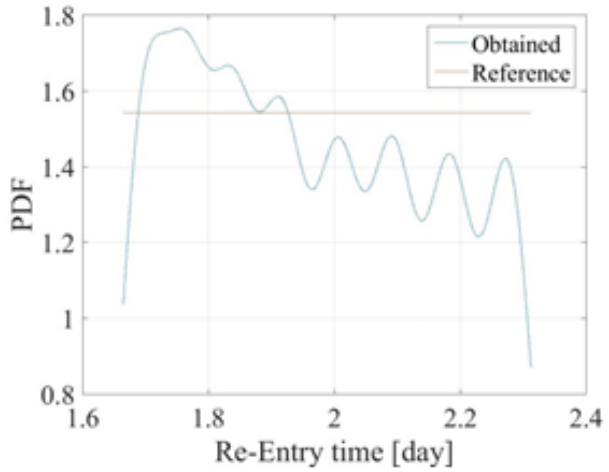

Figure 13: Re-entry time distribution for Case 3

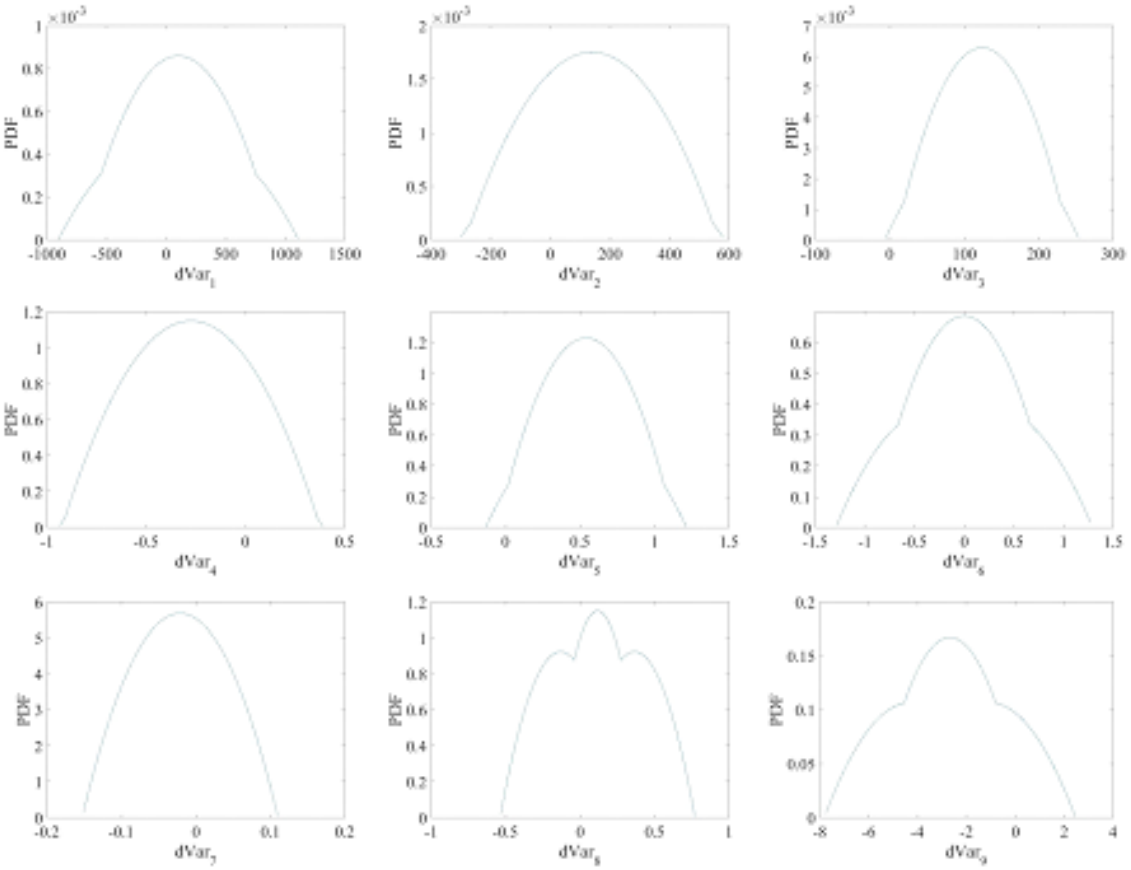

Figure 14: Optimal input distributions for Case 4 (two kernels for each input variable, with the constraint to include the nominal value)

tions of the state variables, instead of time series as classically done. The details are described thereafter.

4.1. Theory

We consider the case in which the state vector $\mathbf{x}$ of the system is known but the dynamic model has some unknown components of the states variables. In the general

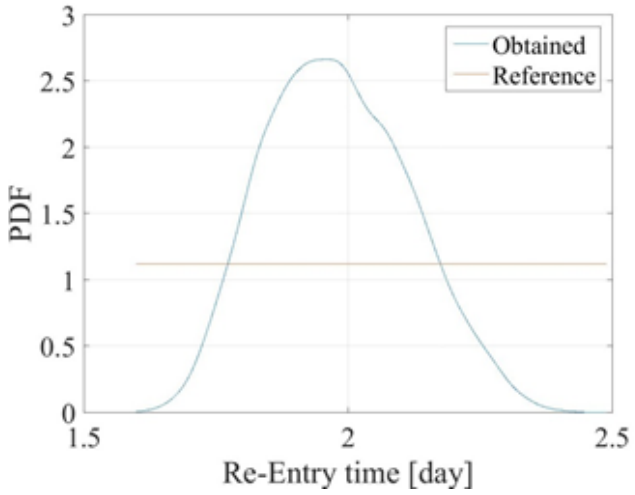

Figure 15: Re-entry time distribution for Case 4

case, one has:

$$\begin{aligned} \frac{\mathrm{d}\mathbf{x}}{\mathrm{d}t}(t) &= p(t,\mathbf{x}(t))f(t,\mathbf{x}(t)) + q(t,\mathbf{x}(t)) \quad \forall t \in [t_0, t_f], \\ \mathbf{x}(t_0) &= \mathbf{x}_0. \end{aligned} \tag{3}$$

where f represents the known model, $p(t,\mathbf{x})$ is a multiplicative unknown function and $q(t,\mathbf{x})$ is an additive unknown function. The two functions p and q can be expressed as a truncated series of the known states and the time with unknown coefficients to be determined from measurements and observations.

Here, we considered the reduced case in which p is fully known and q does not depend on time. The state equation now writes:

$$\frac{\mathrm{d}\mathbf{x}}{\mathrm{d}t} = f(t,\mathbf{x}) + q(\mathbf{x})$$

The proposed approach assumes that: $q = Q$, where Q is a multivariate polynomial function, while the time series approach would assume that q is a univariate polynomial (function of t only). By nature, such a polynomial expansion diverges when t goes to infinity, which means that it can be valid only on a short arc of the trajectory. On the other hand, the state vector is usually bounded (at least it is the case for an orbiting object) and so is $Q(\mathbf{x})$. Additionally, writing the empirical acceleration with respect to the state variables makes it possible to reuse the same function on other time intervals, when $\mathbf{x}$ is still in the same domain.

Typically, for applications to space trajectories, Q has three non-zero components, representing non-modeled terms in the acceleration, hence the name 'empirical acceleration'. As a vector of polynomials, Q is completely defined by its coefficients $c_1, \ldots, c_M$ (that correspond to a given basis, for example the monomials). Therefore, to characterize the empirical acceleration, it is necessary to somehow fit them. Note that the integer M growths exponentially with the order of the expansion D, as:

$$M = \frac{(N+D)!}{N!D!}$$

where N is the dimension of the state e.g. 6 for the position-velocity vector. M evaluations of Q would allow to uniquely determine its coefficients. More would require a

method such as the least square algorithm to derive $c_1, \ldots, c_M$, as the system would have more equations than variables.

Here, it is assumed that only sparse measurements of the state $\mathbf{x}_1, \ldots, \mathbf{x}_S$ are available at times $t_1, \ldots, t_S$. Sparse means that $S < M$. For instance, they can be radar measurements, which require the spacecraft to be in visibility. Typically, they introduce an error $\mathbf{e}$ on the state than can be bounded, between a lower bound $\mathbf{l}$ and an upper bound $\mathbf{u}$: $\mathbf{l} < \mathbf{e} < \mathbf{u}$, with, usually, $\mathbf{l} = -\mathbf{u}$. It is possible to use these measurements to derive the coefficients of Q by solving the following optimization problem (P1):

$$\begin{aligned} &\min J(c_1, \ldots, c_M) \\ &\text{s.t. } \mathbf{l} < \mathbf{x}(t_1) - \mathbf{x}_1 < \mathbf{u}, \\ &\qquad \ldots \\ &\mathbf{l} < \mathbf{x}(t_S) - \mathbf{x}_S < \mathbf{u}. \end{aligned} \tag{4}$$

where $\mathbf{x}(t)$ is the state propagated at time t from the initial condition $\mathbf{x}_0$. In other words, one uses the sparse measurements as path constraints on the simulated trajectory, the latter being a function of the coefficients. The cost J enables to converge to a specific solution among all the feasible ones. A possibility is to use the squared Euclidean norm of the vector $(c_1, \ldots, c_M)$: $J_0 = c_1^2 + \cdots + c_M^2$. Then $c_1 = c_2 = \cdots = c_M = 0$ is the global minimum of J_0, which means that if the model was perfect, one would obtain $q = 0$. It is worth noticing that the search can be simplified by a priori forcing some coefficients to be zero, because it then reduces the number of optimization variables.

An important point is that there can be uncertainty even in the initial state $\mathbf{x}_0$, as it can come from a measurement as well. To tackle this case, one can treat the coefficients $c_1, \ldots, c_M$ as random variables. Knowing the probabilistic distribution of $\mathbf{x}_0$, it is then possible to derive their own distribution. More precisely, by sampling the initial state and computing the coefficients of the empirical acceleration for each sample, one obtains an empirical distribution for $c_1, \ldots, c_M$. The formulation of this problem depends on the state vector $\mathbf{x}$. As a result, the choice of the state variables is paramount. The issue with Cartesian coordinates is that their variation in time is fast. For less oscillation in the empirical acceleration, one would need variables that evolve in a steadier way. Thus here it is proposed to use a different set of coordinates: the so-called modified Hill variables [3, 11], which are defined as:

- r: distance to Earth's center,
- u: argument of latitude,
- h: right ascension of the ascending node,
- v_r: radial velocity,
- v_u: transversal velocity,
- $H = \|\mathbf{G}\| \cos(I)$: projection of the angular momentum $\mathbf{G}$ onto the Z axis of the inertial frame (I is the inclination).

Let (F_r, F_u, F_n) be the radial, transversal and out-of-plane components of the non-Keplerian acceleration in the local orbital frame. Then the equations of motion with the modified Hill variables write [11]:

$$
\begin{aligned}
\dot{r} &= v_r \\
\dot{u} &= \frac{v_u}{r} - F_n \frac{\cos I \sin u}{v_u \sin I} \\
\dot{h} &= F_n \frac{\sin u}{v_u \sin I} \\
\dot{v}_r &= \frac{v_u^2}{r} - \frac{\mu}{r^2} + F_r \\
\dot{v}_u &= F_u - \frac{v_r v_u}{r} \\
\dot{H} &= F_u r \cos I - F_n r \sin I \cos u
\end{aligned}
\tag{5}
$$

Each component of (F_r, F_u, F_n) is the sum of the modeled terms (containing for instance the J_2 contribution, atmospheric drag, etc.) and the unknown one, the corresponding component of Q.

4.2. Test case

This example applies the method described previously to an arc of GOCE's trajectory, using the modified Hill variables as the state vector.

4.2.1. Settings

The case presented here simulates approximately one period of the orbital motion of GOCE (the initial condition is taken on Day 2 of the POD at 00:00). Two measurements are used to compute the polynomial coefficients ($S = 2$): one in the middle of the trajectory and the other one at the end. In order to simplify the optimization problem, the empirical acceleration is assumed to act only in-plane. The radial and transversal components are written as second order polynomial ($D = 2$). In summary, Q writes as follows:

$$
\begin{aligned}
\dot{Q}_r &= c_1 + c_3 r + c_5 r^2 + c_7 r u + c_9 v_r + c_{11} v_r^2 + c_{13} v_r v_u \\
\dot{Q}_u &= c_2 + c_4 u + c_6 u^2 + c_8 r u + c_{10} v_u + c_{12} v_u^2 + c_{14} v_r v_u \\
\dot{Q}_n &= 0
\end{aligned}
\tag{6}
$$

Note that some coefficients in Q_r and Q_u are set to zero heuristically (for example there is no linear term in u in Q_r) so that the total number of unknown is 14. To avoid numerical issues, the state variables are scaled in the following way: distances are normalized with the Earth radius and angles with 2π.

The vectors $\mathbf{u}$ and $\mathbf{l}$ for the measurements are $\mathbf{u} = -\mathbf{l} = [1e-2km, 5e-3rad, 5e-3rad, 1e-3km/s, 1e-3km/s, 1e-2km^2/s]$.

As for the non-Keplerian accelerations already modeled in the dynamics, they account for the high-order terms of the Earths potential up to degree 20 as well as atmospheric drag and lunisolar perturbations (as computed from an early version of the code described in Section 5). As a result, the additive term q can capture additional perturbation terms or potential mismatches in the known model. Furthermore, it has to be remarked that given the uncertainty in the aerodynamic forces, the multiplicative term p can provide further interesting insight in that part of the model. In this test, however, we limit our attention to the additive term as an illustrative example.

4.2.2. Results - Probability distributions

This example is run assuming that the initial conditions are stochastic and follow a uniform distribution in the interval $[\mathbf{x}_0 + \mathbf{l}, \mathbf{x}_0 + \mathbf{u}]$, where $\mathbf{x}_0$ is their nominal occurrence. In the general case the initial conditions are assumed to be coming from and OD campaign and will have a known distribution, possibly Gaussian with known covariance. Out of 1000 samples, 193 led to a convergence of the optimization problem P1, giving as many sets of coefficients $(c_1, c_2, ..., c_{14})$. They are represented in Figure 16 by their mean value ± 1 standard deviation.

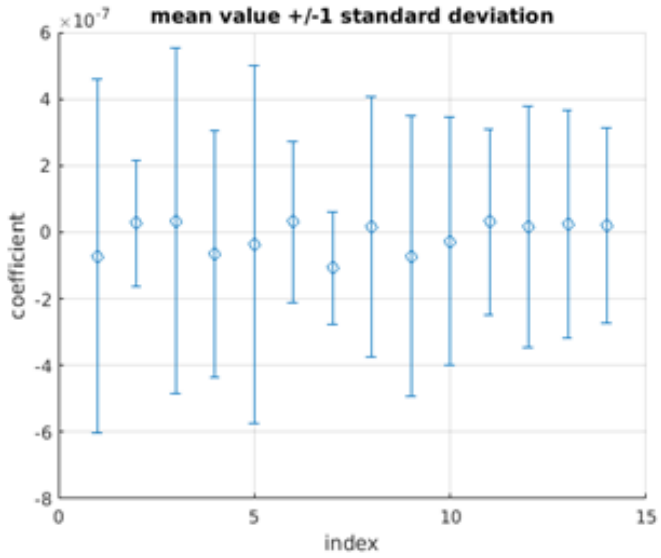

Figure 16: Mean Values and Standard Deviations of Empirical Coefficients

Next, each coefficient's distribution is shown in its integrity (Figure 17 to Figure 23).

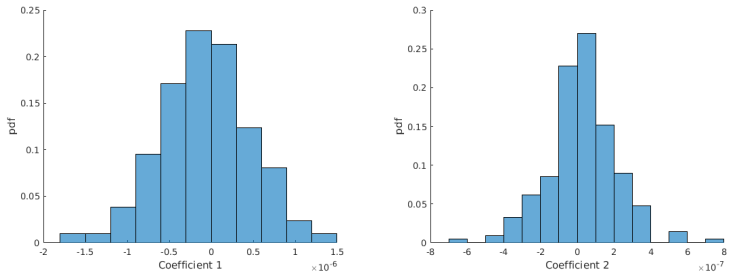

Figure 17: Histograms for Coefficients 1 and 2

The probabilistic distributions of the coefficients can be used to analyze the missing components in the model. In this particular example, one can see that the histograms for coefficients number 5 and 7 are clearly not centered. Moreover, the distributions of c_6 and c_{12} are rather asymmetric. All these features suggest that the corresponding terms in the empirical acceleration capture non-modeled parts of the dynamics. For instance, coefficient number 12 that multiplies the square of the velocity in the transversal component can be interpreted as an imperfect representation in the model of the aerodynamics, due to the large uncertainty in atmospheric density and drag coefficient. Other terms, associated to r and u, are most likely correlated with the high order terms in the gravity potential.

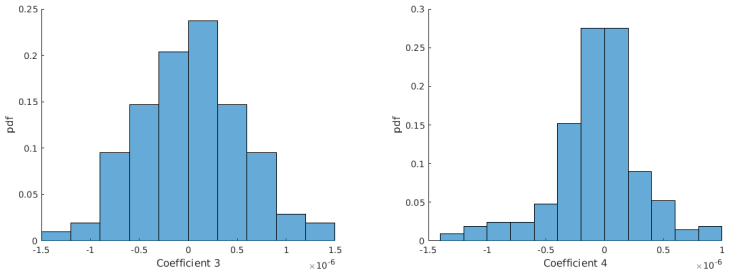

Figure 18: Histograms for Coefficients 3 and 4

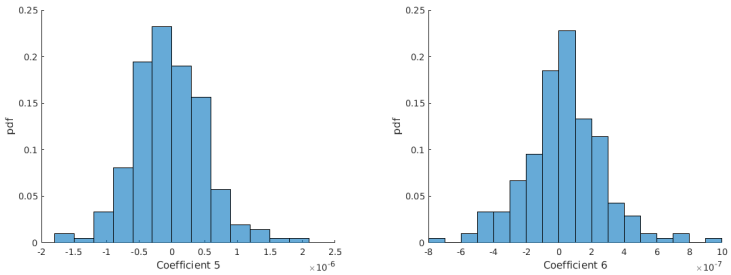

Figure 19: Histograms for Coefficients 5 and 6

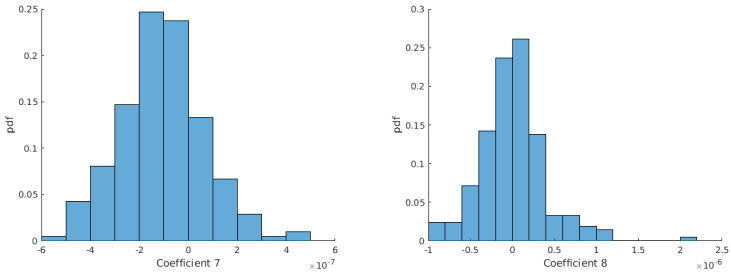

Figure 20: Histograms for Coefficients 7 and 8

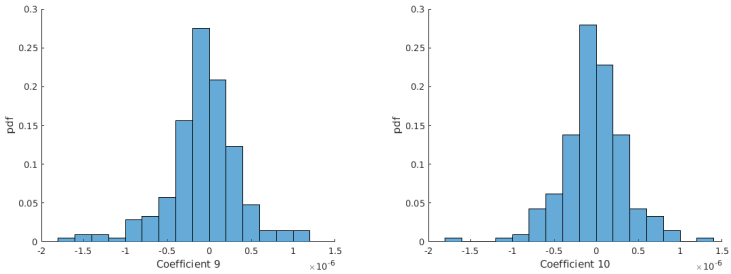

Figure 21: Histograms for Coefficients 9 and 10

4.2.3. Results - Trajectories

There are as many occurrences of the empirical acceleration as there are sets of coefficients. They are all depicted on Figure 24. Recall that, by nature, the out-of-plane contribution is always zero. With this particular formulation of Q_r and Q_u, the former is basically one order of magnitude higher than the latter. Note that this process is not an Orbit Determination, but an identification process aimed at identifying missing parts in the dynamical model. Moreover, the uncertainty on the simulated measurements does not come from real data and is defined with intervals centered on the nominal

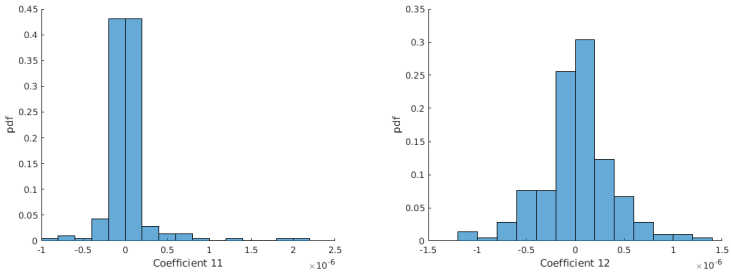

Figure 22: Histograms for Coefficients 11 and 12

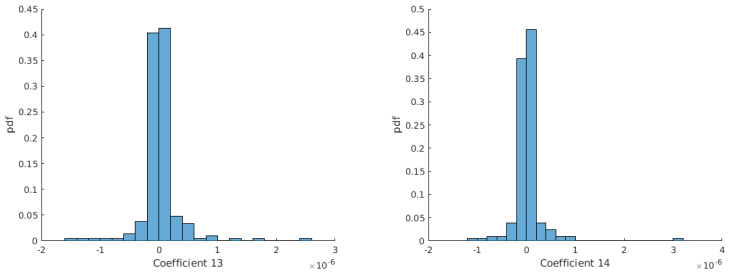

Figure 23: Histograms for Coefficients 13 and 14

Hill variables. The used assumption is that the measurements of the initial states, and any intermediate states, in the radial direction are not very good, and then the process identifies a large radial component of the empirical acceleration.

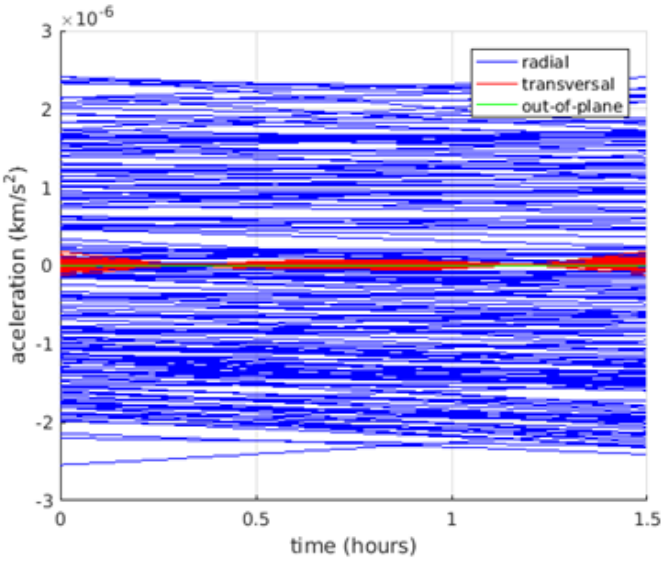

Figure 24: Components of the flux of empirical accelerations

In order to visualize the satisfaction of the path constraints, one can look at the difference between the propagated trajectories and the real one (from the POD), both when the empirical acceleration is on and off. Figures 25 to 30 show, for the six state variables, these differences. On the left hand side, only the mean state (in time) is represented, while the right hand side depicts the whole flux of samples to see the global picture. It is clear that without the empirical acceleration, the trajectories do not pass by the way-points (in red).

In summary, the representation of the empirical acceleration can be done via polynomial functions of the state variables. Accounting for uncertainty can be achieved by considering probabilistic distributions rather than deterministic values of the polynomial coefficients.

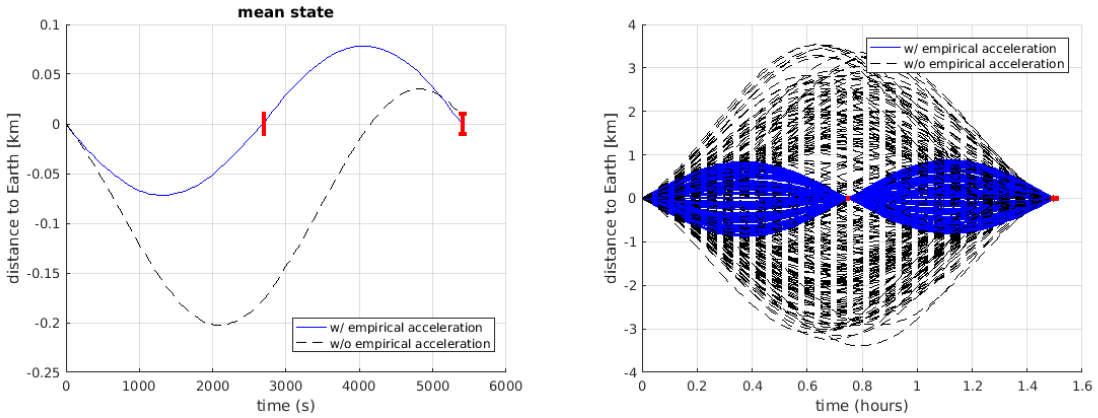

Figure 25: Differences in Hill Variable 1 versus Time with and without the Empirical Acceleration for the mean state (left) and the whole flux of trajectories (right)

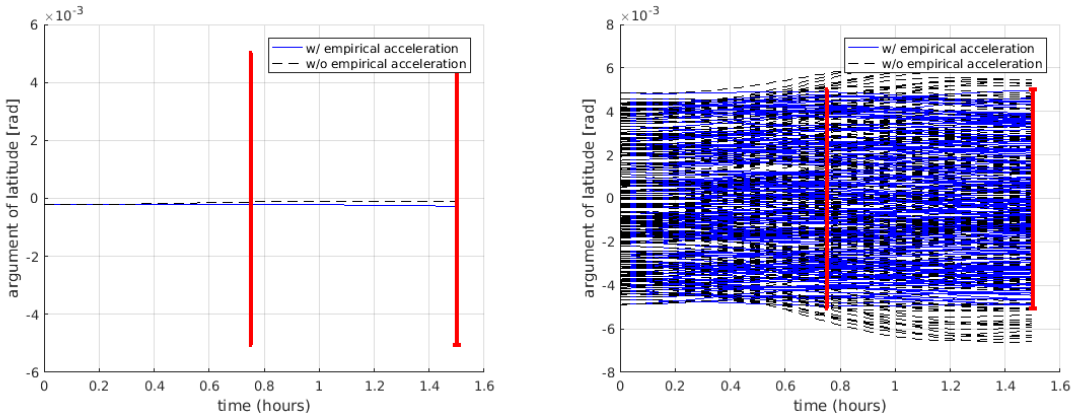

Figure 26: Differences in Hill Variable 2 versus Time with and without the Empirical Acceleration for the mean state (left) and the whole flux of trajectories (right)

4.2.4. Results - Predictions

As mentioned before, an advantage of writing the empirical acceleration as a function of the state variables is that it does not depend directly on time. As a result, it can possibly be reused on time intervals that are different from the one where it had been originally derived, as long as the state lies in the same domain so that no extrapolation is performed. Note that in order to avoid extrapolations due to the argument of latitude u, that grows indefinitely with time, this variable needs to be reset modulo 2π when necessary. To test the aforementioned property, the coefficients computed previously have been reused on a consecutive arc of the trajectory, with a time span of half an orbit. In other words, the goal is to try to reuse the same polynomial for the

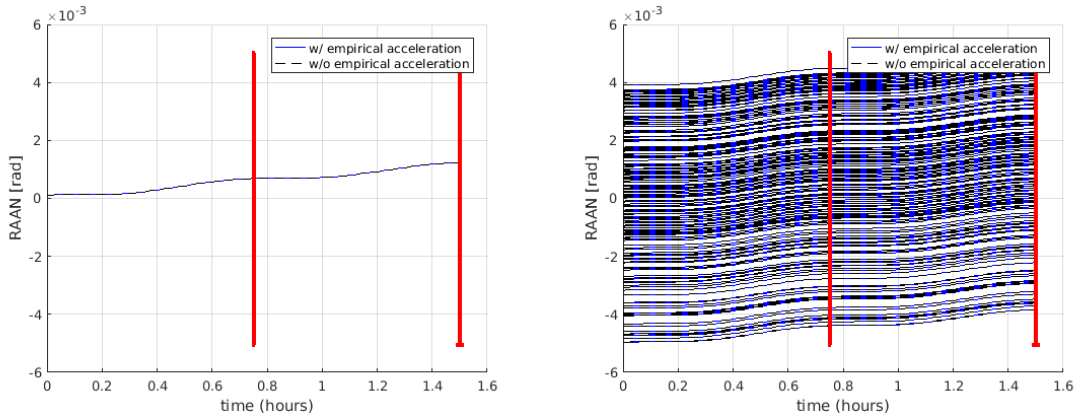

Figure 27: Differences in Hill Variable 3 versus Time with and without the Empirical Acceleration for the mean state (left) and the whole flux of trajectories (right)

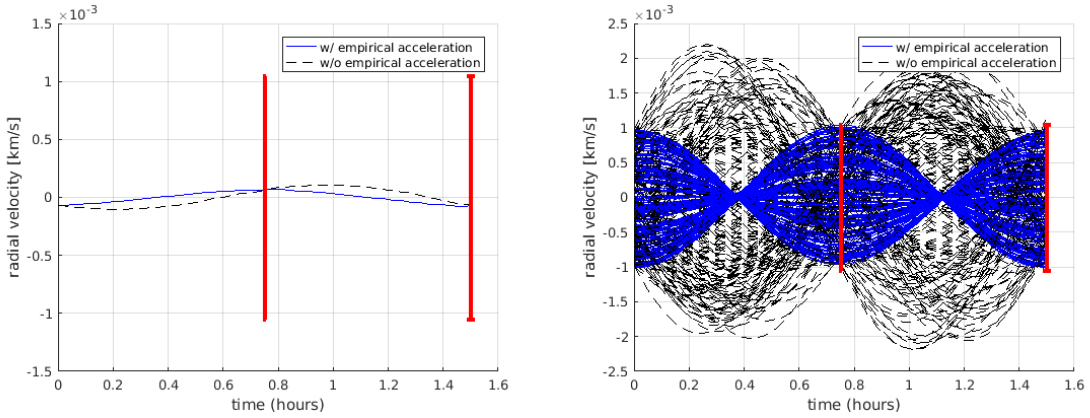

Figure 28: Differences in Hill Variable 4 versus Time with and without the Empirical Acceleration for the mean state (left) and the whole flux of trajectories (right)

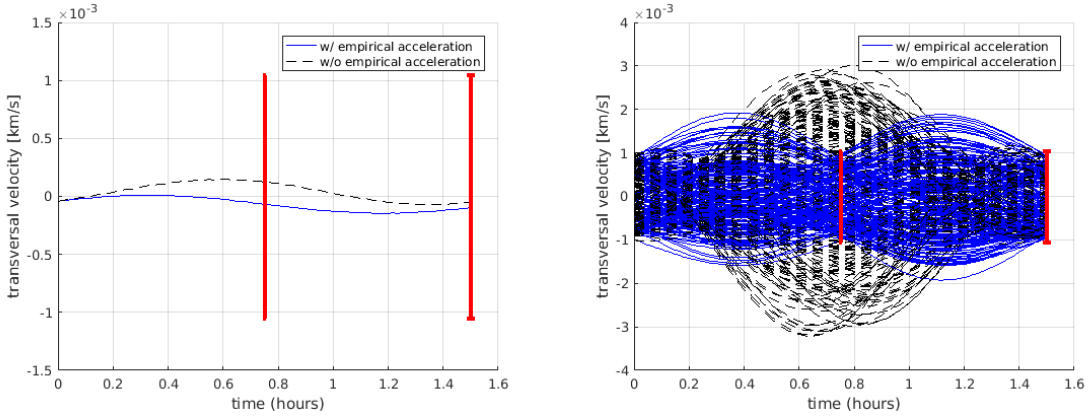

Figure 29: Differences in Hill Variable 5 versus Time with and without the Empirical Acceleration for the mean state (left) and the whole flux of trajectories (right)

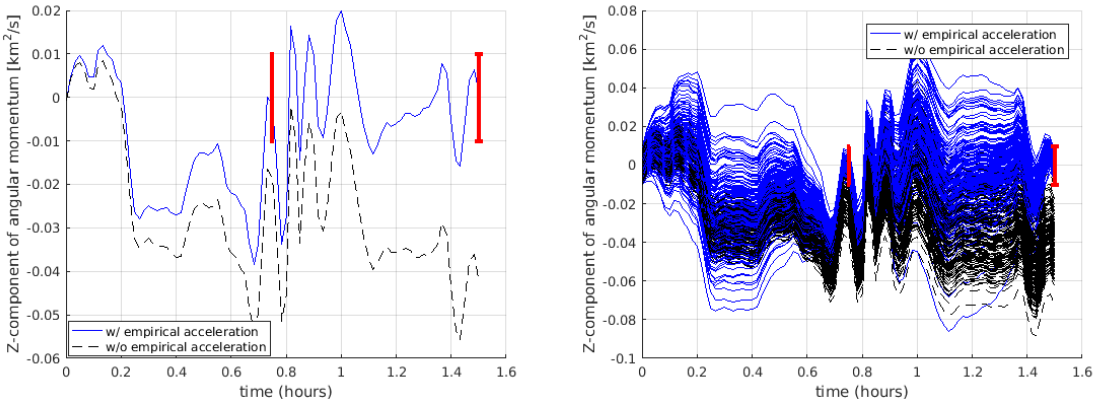

Figure 30: Differences in Hill Variable 6 versus Time with and without the Empirical Acceleration for the mean state (left) and the whole flux of trajectories (right)

empirical acceleration until the next measurement, without using it to modify the coefficients. The same samples than before are propagated over the extra time, both with and without the empirical acceleration. Results are depicted in Figures 31 to Figure 33 for the whole set of initial conditions. For Hill variables number 2, 4 and 5, trajectories under the influence of the empirical acceleration satisfy the constraints, while the uncorrected scenarios go way off limits. For variables 1 and 6, both cases violate the constraints, but it is noticeable that the empirical acceleration brings each sampled trajectory always closer to the way-point. As for the right ascension of the ascending node, it is a bit special and does not really matter as in this example this variable is actually not controlled, due to the chosen expression for the polynomials (no out-of-plane component). These contrasted results are likely due to two things. First, the relatively low number of measurements (only 2) as well as samples used to compute the polynomial coefficients (about 200). Larger statistics should be used to improve robustness, with an obvious increase in computational time. Second, the formulation chosen here to write the empirical acceleration neglects the out-of-plane component and depends only on 4 state variables out of 6, which is somehow restrictive, but on the other hand made the convergence of the optimization process much easier.

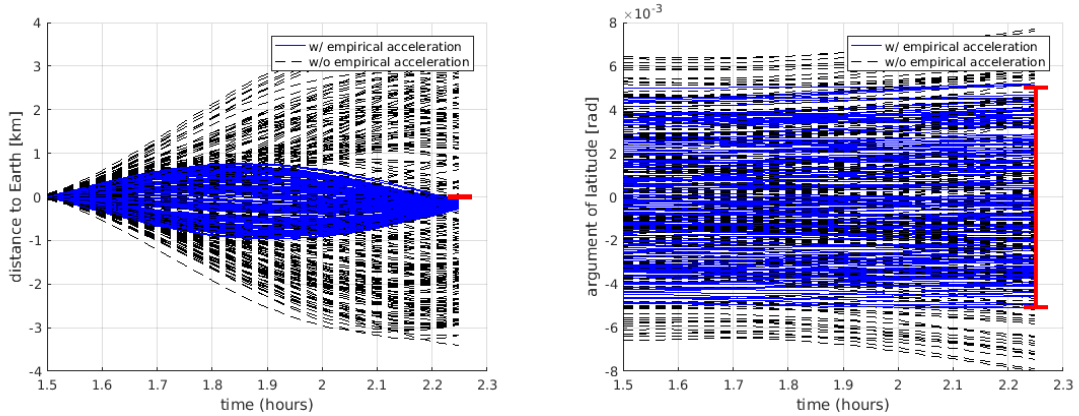

Figure 31: Differences in the Hill variable 1 (left) and 2 (right) vs time, with (blue) and without (black) the empirical acceleration until the following measurement

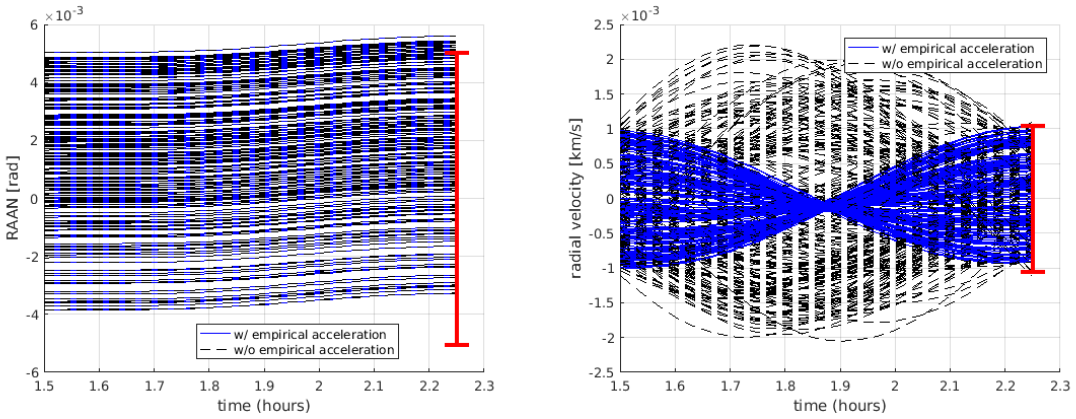

Figure 32: Differences in the Hill variable 3 (left) and 4 (right) vs time, with (blue) and without (black) the empirical acceleration until the following measurement

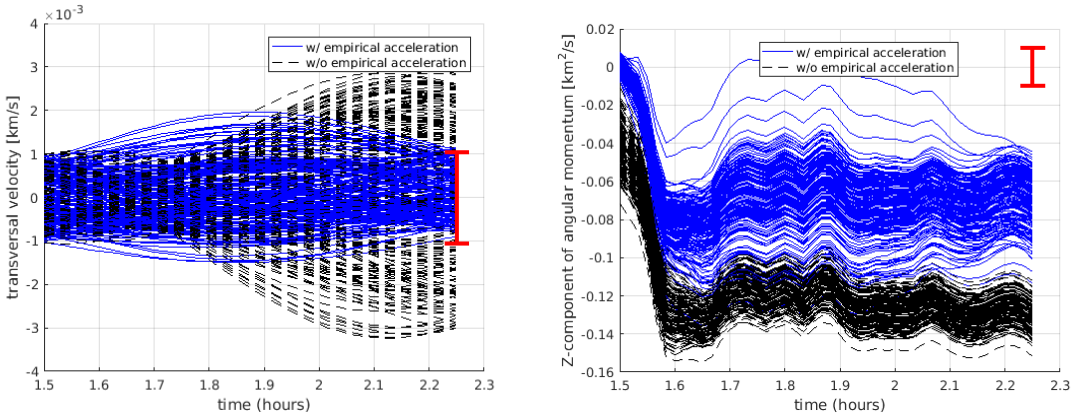

Figure 33: Differences in the Hill variable 5 (left) and 6 (right) vs time, with (blue) and without (black) the empirical acceleration until the following measurement

5. Machine Learning for fast re-entry predictions of GOCE-like objects

As mentioned in Section 2.3, the skew normal probabilistic law, fully described by the independent parameters ξ, ω and α, appears to be a good fit in general for the distributions obtained by simulating GOCE's re-entry with 3DoF. This motivates for predictions of PDF for similar objects by learning the skew-normal coefficients, based on a database of atmospheric re-entry uncertainty campaigns. These distributions are still generated via the AD-HDMR approach. The required samples are computed by running an in-house simulator at Strathclyde University that is described thereafter, before presenting the predictors used and results obtained.

5.1. Re-entry model

For the GOCE-like objects, trajectories have been computed with a code implemented in C++, propagating position and velocity in an Earth-Centered Inertial Frame (ECIF). As this particular study focuses on low altitudes, only gravity and aerodynamics are taken into account. Third-body effects are neglected and the geopotential is expanded at order and degree 36, with coefficients taken from EGM96. Due to the cannonball assumption implied by the 3 degrees-of-freedom, the aerodynamic forces are limited to the drag component, with Jacchia-Gill [7] used as atmospheric model.

The numerical integration, performed with Runge-Kutta-Felhberg 4(5), is stopped at soon as the object reaches an altitude of 80km in the WGS84 system. The parameters associated to drag, namely the mean solar flux $F10.7$, the geomagnetic index Kp and the drag coefficient C_D, are kept constant during each propagation.

As a preliminary test, it has been checked that the newly obtained PDFs were still demonstrating a behavior close to the skew normal law. Such a check is shown on Figure 34. However, it is worth noticing that not all the PDFs are perfectly unimodal. In some cases the related distributions are not similar to any known kernel distributions, as can be seen in Figure 35. Nonetheless, the skew normal distribution still performs better than the other models and gives an acceptable approximation of the PDF. This less standard shape of the data seems to be associated to short re-entry times i.e. within a couple of days. These cases correspond to initial conditions already very low in altitude or to drag parameters whose value causes a significant energy dissipation through aerodynamics.

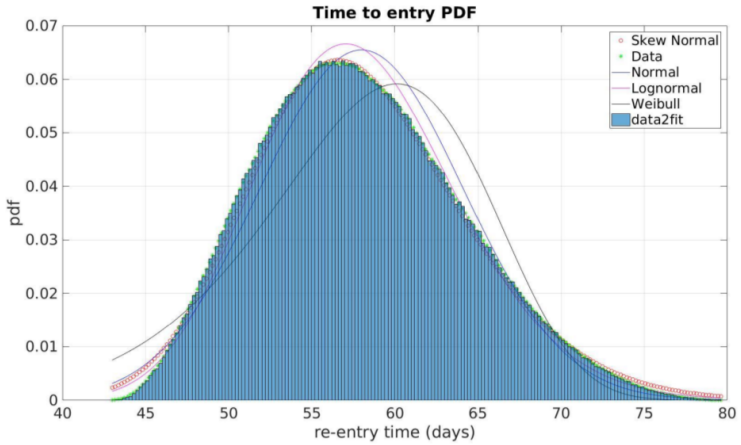

Figure 34: Comparison between data and fitting models in a typical case

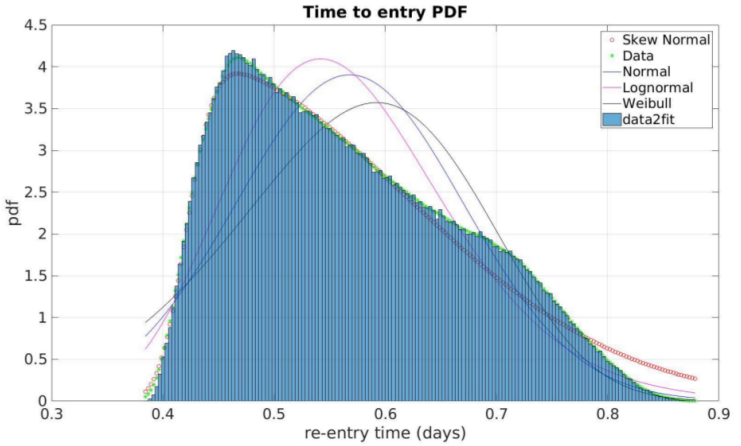

Figure 35: Comparison between data and fitting models in a less favorable case

5.2. Setting and initial conditions

A nominal initial condition corresponding to one of the GOCE states during the second day of the decay phase has been considered:

- **Nominal initial conditions in inertial frame**
  - $\mathbf{r}$ = (-4.938007E+6; 3.146402E+6; 3.060525E+6) [m]
  - $\mathbf{v}$ = (-2.485590E+3; 2.761362E+3; -6.820932E+3) [m/s]
- **Nominal initial conditions (Keplerial elements)**
  - NominalKE = (a=6606535.95 [m], e=0.0016879, i=1.684356 [rad], Ω= 5.656225 [rad], ω=1.055246, th=1.601314)

The investigation has been aimed at sampling and then modeling uncertainty distributions for re-entry cases where the considered objects have

- an initial semi-major axis in the range given at the line 1 of Table 1
- an initial eccentricity in the range given at the line 2 of Table 1
- an initial inclination in the range given at the line 3 of Table 1
- an initial Ω= 5.656225 [rad]
- an initial ω=1.055246
- an initial th=1.601314
- a mass in the range given at the line 4 of Table 1
- a cross-section area in the range given at the line 5 of Table 1
- a drag coefficient, C_D, in the range given at the line 6 of Table 1

the nominal $F10.7$ value is in the range given at the line 7 of Table 1, and the nominal Kp value is in the range given at the line 8 of Table 1, and the range of uncertainties on initial states, C_D, $F10.7$, and Kp as given in the lines 9 to 13 of Table 1.

ID	Lower bounds	Upper bounds	Variable
1	$NominalKE_a - 50km$	$NominalKE_a + 20km$	Initial Semi-major axis
2	$NominalKE_e - 10^{-3}$	$NominalKE_e + 10^{-3}$	Initial Eccentricity
3	$NominalKE_i - 10deg$	$NominalKE_i + 10deg$	Initial Inclination
4	$800kg$	$1200kg$	Mass
5	$1m^2$	$5m^2$	Cross area
6	2	5	C_D
7	112	152	$F10.7$
8	3	4	Kp
9	100	2000	$+/-$ int. uncert. on position (m)
10	0.1	2	$+/-$ int. uncert. on velocity (m/s)
11	0.1	0.3	$+/-$ int. uncert. on C_D
12	10	40	$+/-$ int. uncert. on $F10.7$
13	2	3	$+/-$ int. uncert. on Kp

Table 1: Search space

The search space in Table 1 has been sampled ~ 9300 times. For each sample, an uncertainty propagation campaign via A-HDMR approach has been carried out, and a skew-normal distribution has been fitted to the each corresponding PDF of the re-entry time, and a database with 9300 13-dimensional inputs and 9300 4-dimensional outputs has been created. (Note that the output matrix contains the three coefficients defining the skew-normal, plus a translation term to locate the skew-normal close to the origin). The obtained database has been treated with many different approaches, to build a meta-model directly mapping the variables in Table 1 to the parameters of the skew-normal distribution that best fits the re-entry time PDF.

In particular, the following approaches have been used: Feed Forward Artificial Neural Networks (FF-ANNs) with Bayesian Regularization (BR), with Levenberg-Marquardt (LM), with Adam, and with L-BFGS back-propagations techniques (the latter two methods implemented in Python, while the former three use ©Matlab built-in functions). Moreover, Radial Basis networks, Generalized Radial Basis networks, and the DACE library for Kriging have been also tested.

5.3. Results

The investigation is still ongoing, but on the basis of current results, it can be said that the single layer FF-ANN with BR learning is confirmed as a reliable method having good generalization capabilities, but the learning process is very slow; tested on some random check sample points not belonging to the database it gives reasonably good results both when trained with a local sub set of data (1000 points around the check point), and when trained with the entire database. An example of the performance of first approach is given in Figure 36, where the estimated skew-normal is compared with the one fitted on the PDF obtained with the A-HDMR approach. The same case treated with the FF-ANN-BR considering the entire database is presented in Figure 37.

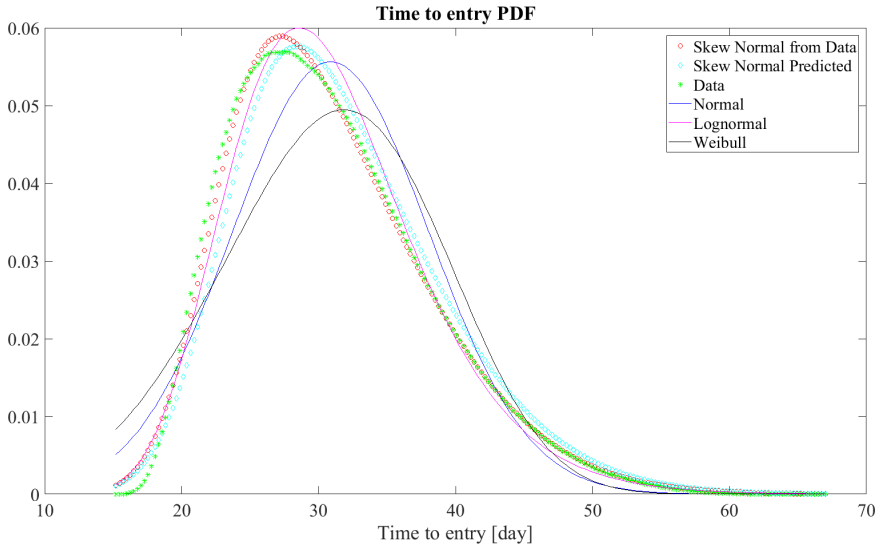

Figure 36: Skew-normal distribution predicted by local FF-ANN-BR (cyan dots) compared to the skew-normal (red dots) fitted on the PDF obtained by the A-HDMR approach (green dots)

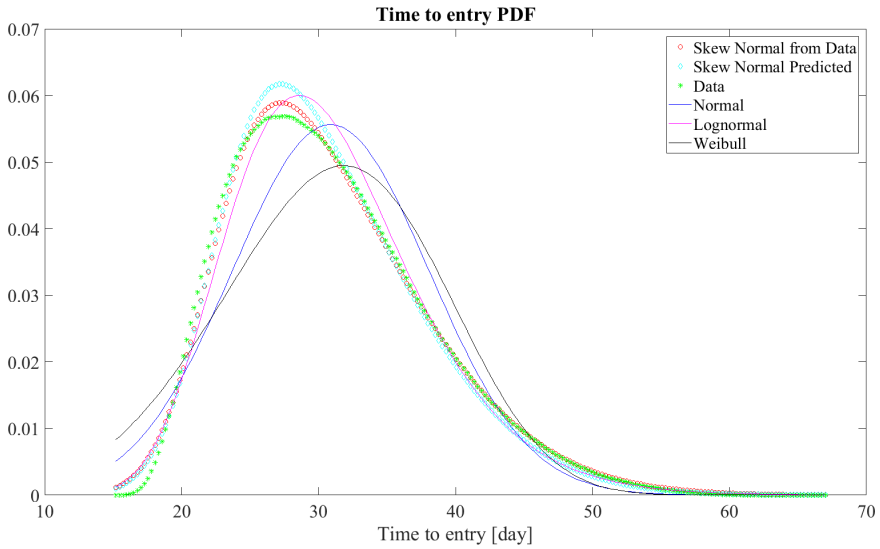

Figure 37: Skew-normal distribution predicted by local FF-ANN-BR (cyan dots) compared to the skew-normal (red dots) fitted on the PDF obtained by the A-HDMR approach (green dots)

6. Conclusion

The paper presents some of the main results and activities to characterize and propagate the uncertainties on the atmospheric re-entry time of GOCE carried out within the framework of an ESA ITT project on benchmarking GOCE's re-entry prediction uncertainties.

Results obtained for the Uncertainty Propagation analyses have pointed out shapes of the PDFs for the re-entry time depending on the degrees of freedom (3 or 6). In particular, when attitude is considered, the function linking the re-entry time to the considered uncertainties of the uncontrolled GOCE can be multi-modal, resulting into a non-standard PDF with multiple peaks. Distributions become unimodal if a single regime (stable or pure tumbling) lasts during most of the re-entry, and in this case distributions obtained via 3DoF propagation can match relatively well the ones obtained with the 6DoF propagation.

Two different uncertainty quantification/characterization approaches have been also proposed. The same interpolation techniques used for computationally cheap, non-intrusive methods for UP, allowed the development of two methods based on direct optimization approaches, namely the Boundary Set Approach and the Inverse Uncertainty Quantification. Both have been tested, but not fully exploited. Most of the test analyses were carried out by using approximated UP techniques, but there is still no information on the output distribution to match.

Moreover, a new approach to empirical acceleration has been tested on arcs of GOCEs trajectory. Instead of a time series, the function is written as a multivariate polynomial, whose variables are the components of the state vector. There is a gain in generality as the polynomial coefficients derived from measurements are less time-dependent. Here, the modified Hill variables were used to represent the state, as most of them vary slowly with time. Calculating the coefficients of the empirical acceleration is done via an optimization process, where the trajectory is constrained to pass through way-points given by the measurements. Thus, the results are highly dependent on the

parameters of the problem (number of coefficients, tightness of the box constraints, etc.). Uncertainty in the initial conditions is handled by computing as many sets of coefficients as there are samples. Analyzing the resulting probability distributions then helps to understand where the missing components of the dynamical model lye.

Finally, some preliminary results on the use use of meta-modeling techniques to directly map a range of initial states and model uncertainties into re-entry time windows distributions, providing with a very fast characterization of the output PDF not requiring any propagation at all. Preliminary results shown in this paper tend to confirm that this is possible, but the approach should be better implemented and further tested in the future.

Follow-up work includes: 1) the use of a more complex model for the uncertainty acting on the atmospheric parameters: more precisely, instead of having them constant during each propagation, one could allow variations over time following some probabilistic law; 2) the finalization of the meta-modeling approach to learn the coefficients of the skew-normal distributions; and 3) the exploration of the use of the same meta-modeling techniques to learn the re-entry dynamics and map the initial conditions and the object and atmosphere properties to the re-entry time.

Acknowledgments

This work was carried out under ESA Contract No. 4000115172/15/F/MOS Benchmarking re-entry prediction uncertainties. The support of the ESA Space Debris Office is gratefully acknowledged. The authors are particularly thankful to Stefano Cicalò, James Beck and Ian Holbrough for their precious comments and suggestions during the project.

The authors also acknowledge the use of the 3DoF and 6DoF propagators of Belstead Research Ltd for the analyses presented in Section 2 , and the EPSRC funded ARCHIE-WeSt High Performance Computer (www.archie-west.ac.uk). EPSRC grant no. EP/K000586/1.

References

[1] R. Armellin, P. Di Lizia, F. Bernelli-Zazzera, and M. Berz. Asteroid close encounters characterization using differential algebra: the case of apophis. *Celestial Mechanics and Dynamical Astronomy*, 107(4):451–470, 2010.

[2] J. Beck, I. Holbrough, M. Vasile, E. Minisci, and R. Serra. Debris evolution uncertainty quantification. UKSA NSTP Pathfinder Final Report, December 2016.

[3] I. G. Izsak. A note on perturbation theory. *The Astronomical Journal*, 68:559–561, 1963.

[4] M. Kubicek, E. Minisci, and M. Cisternino. High dimensional sensitivity analysis using surrogate modeling and high dimensional model representation. *International Journal for Uncertainty Quantification*, 5(5):393–414, 2015.

[5] P. M. Mehta, M. Kubicek, E. Minisci, and M. Vasile. Sensitivity analysis and probabilistic re-entry modeling for debris using high dimensional model representation based uncertainty treatment. *Advances in Space Research*, 59(1):193–211, 2017.

[6] E. Minisci and M. Vasile. Adaptive inflationary differential evolution algorithm. In *Congress on Evolutionary Computation (CEC2014)*, 2014.

[7] O. Montenbruck and E. Gill. Satellite orbits. *Springer*, 2, 2000.

[8] C. Ortega Absil, R. Serra, A. Riccardi, and M. Vasile. De-orbiting and re-entry analysis with generalised intrusive polynomial expansions. In *67th International Astronautical Congress*, 2016.

[9] C. Tardioli, M. Kubicek, M. Vasile, E. Minisci, and A. Riccardi. Comparison of non-intrusive approaches to uncertainty propagation in orbital mechanics. In *Proceedings of AAS/AIAA Astrodynamics Specialist Conference, Vail, Colorado*, 2015.

[10] M. Vasile, E. Minisci, R. Serra, J. Beck, and I. Holbrough. Analysis of the de-orbiting and re-entry of space objects with high area to mass ratio. In *Proceedings of AAS/AIAA Astrodynamics Specialist Conference, Long Beach, California*, 2016.

[11] M. Vasile, C. Tardioli, A. Riccardi, and H. Yamakawa. Collision avoidance as a robust reachability problem under model uncertainty. In *Proceedings of 26th AAS/AIAA Space Flight Mechanics Meeting*, 2016.

[12] M. Vetrisano and M. Vasile. Analysis of spacecraft disposal solutions from lpo to the moon with high order polynomial expansions. *Advances in Space Research*, 60(1):38–56, 2017.